Engineered Science

RESEARCH PAPER View Article Online

Robust Construction of Flexible Bacterial Cellulose@Ni(OH)$_2$ Paper: Toward High Capacitance and Sensitive H_2O_2 Detection

Jie Cai[1,2,3,*], Wei Xu[1], Yuheng Liu[1], Zhenzhou Zhu[1,2,3], Gang Liu[1,2,3*], Wenping Ding[1,2,3*], Guozhen Wang[1,2,3], Haibo Wang[4] and Yangchao Luo[5]

Multifunctional properties, including energy storage and sensitive diagnosis, are highly demanded for high-performance supercapacitors and sensors. Herein, we describe a facile method for the synthesis of a multitasking bacterial cellulose@Ni(OH)$_2$ paper for use as a flexible supercapacitor electrode with excellent energy storage performance and a sensing platform for high-sensitivity detection of H_2O_2. Monodispersed surfactant-free Ni(OH)$_2$ particles with a large fraction of edge sites were anchored on the cellulose fiber network, providing a bendable, freestanding, and hydrophilic material, and leading to attractive electrochemical properties. As expected, this flexible electrode exhibited a remarkable areal capacitance of ~2047 mF cm^{-2} and high flexibility allowing it to be bent to arbitrary angles. As a nonenzymatic H_2O_2 detection electrochemical electrode, it displayed a fast amperometric response with a linear range of 0.1–12.4 mM, acceptable sensitivity (~3.79 uA mM^{-1} cm^{-2}), and low detection limit (~0.28 μM, S/N=3). The versatility of the electrode can be demonstrated by its high selectivity in the presence of interfering species, good reliable detection, and also its ability to detect H_2O_2 in real samples. The simple, low-cost, and general strategy presented herein can be extended to the preparation of other biomass materials and open up new opportunities for flexible electronic devices.

Keywords: Bacterial cellulose; Electrode; Flexible supercapacitor; H_2O_2 sensor

Received 17 December 2018, **Accepted** 4 January 2019

DOI: 10.30919/es8d669

1. Introduction

The increasing risks of energy shortage, environmental pollution, and food safety have accelerated new developments in science and technology. In particular, the exploration of nanomaterials with multifunctional applications for the realization and enhancement of energy storage–conversion and contaminant/noxious substance monitoring has attracted the attention of scientists worldwide. A recent literature survey demonstrated that electrode materials using electrochemical effects possess supercapacitive properties and molecular sensing abilities.[1-3]

Electrochemical energy storage provides a promising technology for solving the future energy crisis of the world.[4] As one of the most important energy storage devices, supercapacitors, also called electrochemical capacitors or ultracapacitors, can deliver high power, exhibit fast rates of charge/discharge, and have long lifespans for storing and releasing energy based on nanoscopic charge separation at the interface between the electrode and electrolyte. Thus, supercapacitors will play an essential role in the conservation of exhaustible natural resources and reduction of environmentally hazardous pollutants. Supercapacitors are generally classified into two types based on their charge storage mechanism: electrochemical double layer capacitances (EDLCs) (relies on ion adsorption) and pseudocapacitors (relies on fast surface redox reactions).[5] There have been continuous efforts to determine the effects of electrode materials on the electrochemical performances of supercapacitors. In this regard, a primary research focus is developing different strategies to prepare high-performance electrode materials. Many scientists have studied supercapacitors based on various electrode materials, which are primarily divided into carbon-based materials, conducting polymer materials, and transition metal oxides/hydroxides. In fact, carbon-based materials have been used thus far in supercapacitors because of their high surface areas, including graphene,[6] activated carbon,[7] carbon nanotubes,[8] templated carbons,[9] carbon nanofibers,[10] carbon cages,[11] carbon quantum dots,[12] and carbon foams.[13] We and other researchers have reported that heteroatom-functionalized carbon materials with enhanced special capacitances are promising electrodes for supercapacitors.[14-17] In conducting polymeric materials (e.g., polypyrrole,[18] polyaniline,[19] and polythiophene and its derivatives[20,21]) the reduction–oxidation process occurs at the electrochemical electrodes of pseudocapacitor devices to store and release charge. Self-supported, hollow, porous capsular polypyrrole fibers as a binder-free pseudosupercapacitor electrode material with high capacitance and cycling stability were successfully developed in our previous study.[22] Metal oxides/hydroxides, such as RuO_2,[23] NiO,[24] MnO_2,[25]

[1] *School of Food Science and Engineering, Wuhan Polytechnic University, Wuhan 430023, China*
[2] *Key Laboratory for Deep Processing of Major Grain and Oil (Wuhan Polytechnic University), Ministry of Education, China*
[3] *Hubei Key Laboratory for Processing and Transformation of Agricultural Products (Wuhan Polytechnic University), Wuhan 430023, China*
[4] *School of Chemical and Environmental Engineering, Wuhan Polytechnic University, Wuhan 430023, China*
[5] *Department of Nutritional Sciences, University of Connecticut, Storrs, CT 06269, USA*
***E-mail:** caijievip@hotmail.com, caijievip@whpu.edu.cn (J. Cai); lg820823@163.com (G. Liu); whdingwp@163.com (W. P. Ding)*

CoO, [26] and $Co(OH)_2$ [27] are outstanding electrode materials that can be used to construct high-energy and high-power supercapacitor devices, as they possess high theoretical capacitances. Among these pseudocapacitive materials, $Ni(OH)_2$ is of great scientific interest and is an attractive candidate for high-performance supercapacitors based on its well-defined redox activity, various morphologies, good cost–benefit ratio, environmental friendliness, availability, and high chemical/thermal stability. In our previous work, $Ni(OH)_2$ synthesized on the surface of carbon nanofibers through a solid-state reaction significantly increased the electrochemical performance of the matrix material as a supercapacitor electrode.[14]

In addition to energy storage, electrochemical sensors composed of electrode materials are of practical importance for the reliable detection of contaminants/noxious substances in various areas, such as food, pharmaceuticals, environment, clinical analysis, and biological processes.[28-32] Hydrogen peroxide (H_2O_2) is a common and important chemical compound, which has been widely used in many areas as an oxidizer, bleaching agent, and disinfectant. The detection of H_2O_2 concentration has become critically important because of its ability to induce oxidative damage and apoptosis. Various techniques, colorimetric,[33] titrimetric, fluorescence,[34] chemiluminescence,[35] and electrochemical [36] methods, have been developed to detect H_2O_2. Among the many different approaches, scientists have focused more on the electrochemical method because it is accurate, sensitive, rapid, and convenient. There are two categories of electrochemical H_2O_2 sensors, enzymatic and nonenzymatic, depending on whether enzymes are present or not. Enzymatic H_2O_2 sensors are usually set up by anchoring redox enzymes (e.g., horseradish peroxidase) on the surface of electrode materials to record the redox reaction of H_2O_2 in the form of an electronic current. Enzymatic sensors have exhibited impressive sensitivity and selectivity for H_2O_2 detection. However, these sensors have intrinsic drawbacks associated with their susceptibility to ambient conditions (e.g., humidity, temperature, and pH), and difficultly in purifying enzymes, with their instabilities and complicated immobilization processes limiting their long-term applications. Due to the shortcomings of enzymatic sensors, considerable efforts have been made on the development of non-enzymatic H_2O_2 sensors fabricated using various special electrode materials. To date, non-enzymatic sensors based on metals and their derivatives, such as Co, [37] Cu-Ni,[38] and MoS_2[39] have drawn increasing attention and have been frequently employed to produce H_2O_2 sensors due to their many advantages, including their excellent electrocatalytic reduction activities and high stabilities. Recently, decorating $Ni(OH)_2$ on substrates as electrodes has yielded impressive performances and is a popular strategy to develop efficient electrochemical sensors.

Studies on the various aspects of $Ni(OH)_2$-based electrode materials for supercapacitors or non-enzymatic H_2O_2 sensors have resulted in many improvements above the fields. The increasing number of practical applications has boosted the development of dual-functional $Ni(OH)_2$-based electrodes for high-performance supercapacitors and the efficient detection of H_2O_2 in real samples. Moreover, flexible electronic devices have shown great promise in many applications and have experienced

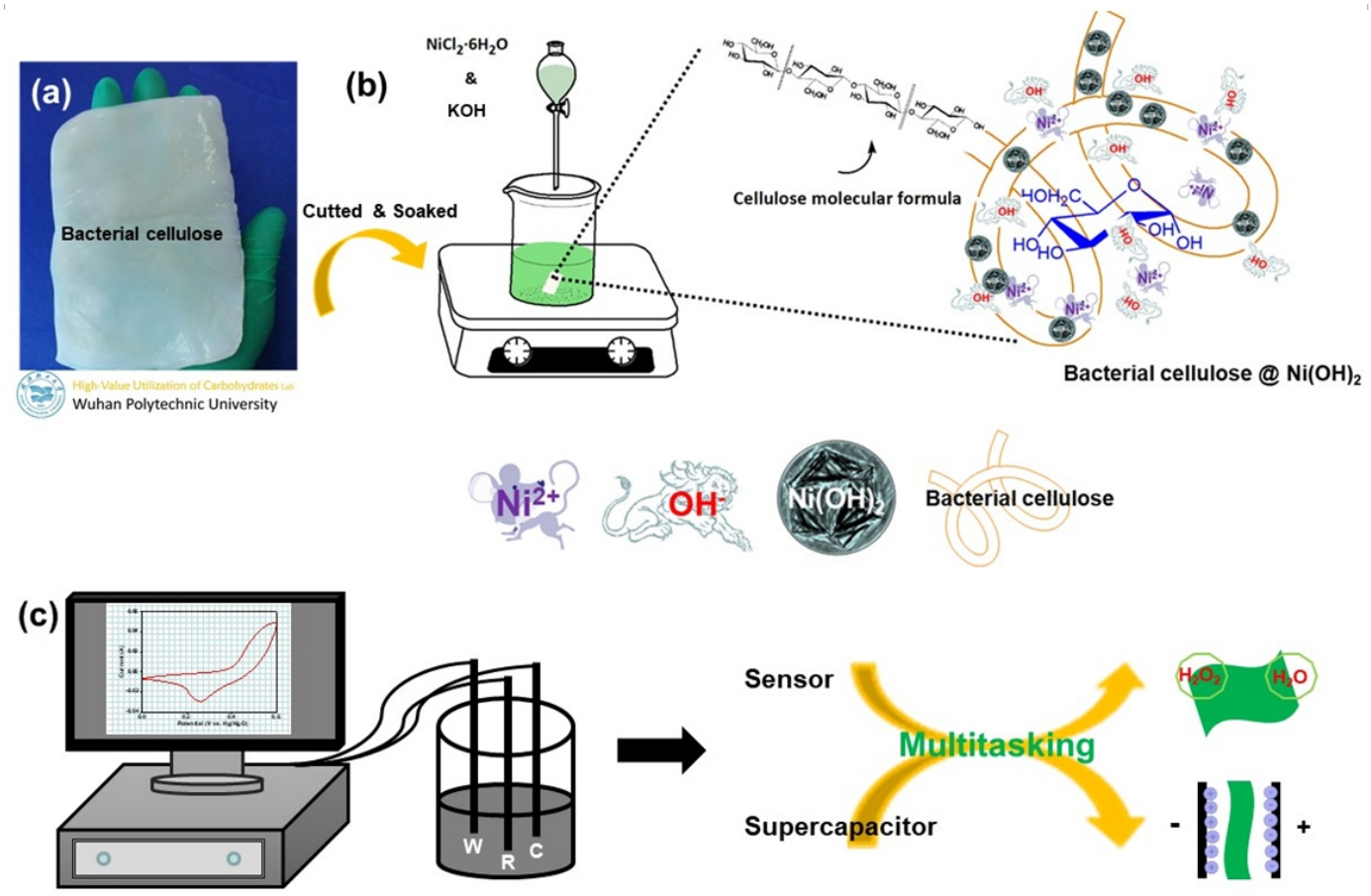

Fig. 1 a) Typical photograph of BC. b) Schematic representation of the in situ chemical precipitation method used for the synthesis of the BC@$Ni(OH)_2$ paper. c) Electrochemical measurements of the BC@$Ni(OH)_2$ electrode and its applications as a H_2O_2 sensor and supercapacitor.

rapid development, for example, as wearable supercapacitors and flexible electrochemical sensors. The hydrophilicity of the electrode matrices promotes the contact of the material with water-soluble media, producing larger and faster responses for improving the electrochemical properties. The integration of the $Ni(OH)_2$-active materials with mechanically tough and hydrophilic bacterial cellulose (BC) (Fig. 1a) substrates is a promising strategy.

Herein, we demonstrated the robust construction of flexible $Ni(OH)_2$-based paper electrodes by simple in situ solution synthesis of $Ni(OH)_2$ on a BC matrix such that $Ni(OH)_2$ particles were anchored on the cellulose fiber network, providing a bendable, freestanding, and hydrophilic material. The BC@$Ni(OH)_2$ paper was a proof-of-concept for flexible electronic devices with dual functions as a supercapacitor electrode material and electrochemical sensor. The noteworthy improvement in the electrochemical capacitive behavior and electrocatalytic oxidation of H_2O_2 was due to the synergistic effect derived from the correlation of the physicochemical properties of the BC@$Ni(OH)_2$ hybrid, which shows promise for applications in the development of flexible supercapacitors and nonenzymatic sensor devices, and the scalable fabrication method will pave the way toward the practical use of these devices.

2. Experimental section

2.1 Reagents and Materials

Bacterial cellulose (BC) was provided by Beijing Guanlan Technology Co., Ltd. (Beijing, China). Nickel chloride hexahydrate ($NiCl_2{\cdot}6H_2O$) was obtained from Sigma-Aldrich (USA). Sodium hydroxide (NaOH) and potassium hydroxide (KOH) were purchased from Sinopharm Chemical Reagent Co., Ltd. (Shanghai, China). Sodium chloride (NaCl), ascorbic acid (AA), uric acid (UA), dopamine (DA), and L-cysteine (L-Cys) were supplied by from Aladdin Industrial Co., Ltd. (Shanghai, China). All reagents were of analytical purity grade and were used directly for the experiments without any further purification.

2.2 In situ synthesis of BC@$Ni(OH)_2$ paper

BC@$Ni(OH)_2$ paper was prepared through an in situ chemical precipitation technique (Fig. 1b). Typically, 1g $NiCl_2{\cdot}6H_2O$ was dissolved in deionized water (50 mL) under intense stirring. Subsequently, a BC pellicle was immersed in the above solution and stirred for 24 h to reach a saturated adsorption state. It was subsequently taken out and soaked into a 50 mL aqueous solution of KOH with the same concentration as the reaction reagent based on the following chemical reaction:

$$NiCl_2{\cdot}6H_2O + 2KOH \longrightarrow Ni(OH)_2 + 2KCL + 6H_2O$$

After the reaction, the as-synthesized sample was collected by centrifugation and washed with distilled water and absolute alcohol several times and dried in a vacuum oven at 80 °C for 12h, after which the BC@$Ni(OH)_2$ flexible paper was obtained.

2.3 Materials characterization

Surface morphology was investigated on a Hitachi S-3000N field emission scanning electron microscope (FE-SEM). Fourier transform infrared (FTIR) spectra were obtained using a NEXUS670 FTIR spectrometer (Thermo-Nicolet, Madison, WI) in specular mode with a resolution of 4 cm^{-1}. X-ray photoelectron spectroscopy (XPS, Axis Ultra DLD) was performed to investigate the surface elemental compositions. The crystallographic information was measured using X-ray diffraction (XRD, PANalytical Empyrean) equipped with Cu-Ka radiation in a 2θ range from 10° to 70°. Thermogravimetric analysis (TGA) was performed using a METTLER TOLEDO TGA/DSC/1100SF instrument under a N_2 atmosphere with a heating rate of 10°C/min in the temperature range of 30 – 800°C. The electrochemical parameters were measured using an electrochemical analyzer system CHI660E (Shanghai, China) (Fig. 1c).

3. Results and discussion

The facile strategy for the fabrication of green colored crystals of $Ni(OH)_2$ anchored on the BC matrix utilizes a chemical precipitation method, and the schematics of the synthesis of the BC@$Ni(OH)_2$ paper are shown in Fig. 1b. The dried BC membrane (Fig. 2a) was first immersed in a $NiCl_2{\cdot}6H_2O$ solution to bring the guest Ni^{2+} ions into the three-dimensional (3D) network structure of BC matrix and achieve an adsorption equilibrium in the nanopores of BC. Promoted by the electrostatic interactions between Ni^{2+} and cellulose, the Ni^{2+} ions adhered to the surfaces of BC fibers, which prevented them from being removed by water during washing. As the process progressed, the color of BC membrane transformed from white to pale green (Fig. 2b), corresponding to the steady adsorption of Ni^{2+} on the membrane. When the membrane was transferred into KOH solution, $Ni(OH)_2$ particles were quickly produced and strongly adhered to the BC fibrous structure due to the strong interaction between Ni^{2+} and OH^-. Finally, the BC@$Ni(OH)_2$ paper was successfully fabricated and its color changed to green promptly (Fig. 2c). As expected, the composite paper could be bent to different angles (Fig. 2d) and rolled from 0° to 180° (Fig. S1, Supplementary Information), indicating that the obtained BC@$Ni(OH)_2$ paper had a high mechanical integrity upon bending and folding. This provided a simple, efficient, and cost-effective approach to prepare flexible and freestanding electrodes that can be used in practical applications.

The morphologies and structures of the pristine BC and BC@$Ni(OH)_2$ paper were investigated by SEM, the images of which are shown in Fig. 2. BC possessed a porous 3D fibrous network with an average fiber diameter less than 100 nm (Fig. 2e). The cross-linked and overlapping structure enhanced the adsorption and distribution of Ni^{2+} on the BC matrix and provided sites for the Ni salt reaction while the fibers anchored and supported the particles that formed. Furthermore, the structure possessed a high surface area and provided adequate space to ensure that the electrolyte ions could permeate into the membrane easily. However, it can be seen from the SEM image of the composite that the foreign particles strongly bound to the substrate were present on the surfaces and in the voids of the fibers, resulting in grooves, wrinkles, and roughness. From these results, it is clear that the deposition of $Ni(OH)_2$ onto the BC membrane successfully and easily produced the BC@$Ni(OH)_2$ hybrid. The EDS spectrum of the BC@$Ni(OH)_2$ paper further confirmed the presence of $Ni(OH)_2$ on the BC substrate (Fig. S2, Supplementary Information). Because of the high hydrophilic BC substrate, the as-fabricated BC@$Ni(OH)_2$ paper also shows hydrophilic with the contact angle less than 60^o (Fig. S3, Supplementary Information).

More detailed information on the chemical composition of the materials was obtained using FTIR, XRD, and XPS. From the FTIR spectrum of BC[40, 41] plotted in Fig. 3a, broad bands at ~3412 and ~2917 cm^{-1} are attributed to the –OH stretching vibrations of hydrogen-bonded hydroxyl groups and the C–H and CH_2 asymmetric stretching vibrations, respectively, whereas the peak at ~1163 cm^{-1} is assigned to the C–O antisymmetric bridge stretching. The strong and sharp bands situated at ~1059 and ~1113 cm^{-1} can be ascribed to the skeletal vibration of functional groups of C–O–C and the C–O pyranose ring,

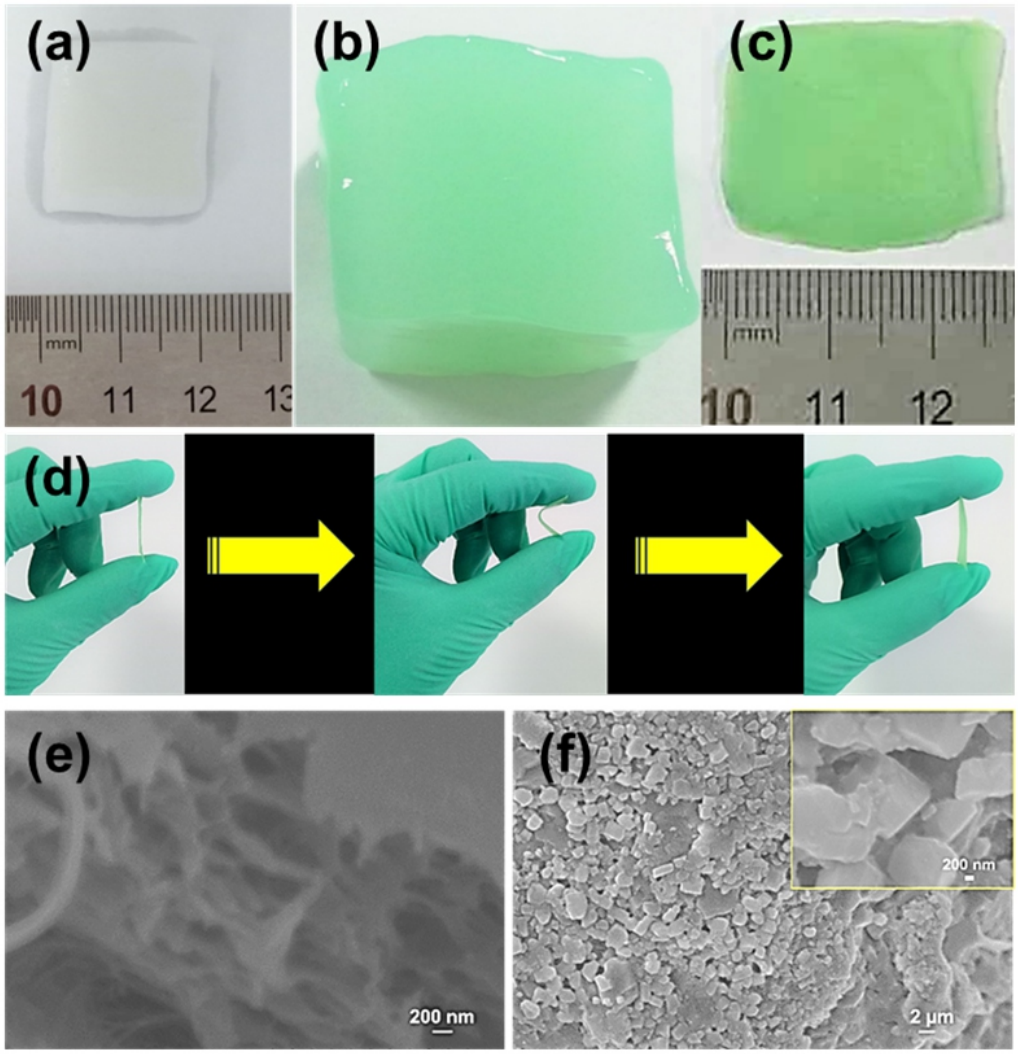

Fig. 2 a-b) Optical images of the derived BC (a), Ni^{2+}@BC (b), and BC@$Ni(OH)_2$ paper (c), and flexibility of bending of BC@$Ni(OH)_2$ paper (d). e-f) SEM images of BC (e) and BC@$Ni(OH)_2$ paper (f).

respectively. These bands in the spectrum of the BC@$Ni(OH)_2$ paper indicate that there were -OH, C-H, and C–O–C groups, which are typical features of BC. The relatively strong OH deformation and bending vibrations may be due to an interaction between the OH groups and the Ni^{2+} ions from the in situ synthesis. However, the narrow and sharp peak located at ~3640 cm^{-1} is attributed the stretching vibrational mode of non-hydrogen-bonded, free OH groups in the $Ni(OH)_2$ structure.[42] Aside for the appearance of the typical peaks of the BC, the spectrum of the BC@$Ni(OH)_2$ composite shows two absorption bands at around 704 and 518 cm^{-1} that are characteristics of δ_{OH} vibrations of hydroxyl groups and the Ni–O vibrations and Ni–O–H bending from $\nu_{Ni\text{-}OH}$, respectively,[43] further confirming the loading of $Ni(OH)_2$ in BC. Fig. 3b shows the XRD patterns of the BC and BC@$Ni(OH)_2$ composite samples. The typical diffraction peaks of neat BC at angles abound 14.8°, 16.7°, and 23.0° are assigned to (10$\bar{1}$), (10$\bar{1}$), and (002), corresponding to the signals of the Cellulose I allomorph.[44] After the reaction, the sample consisted of the well-crystallized $Ni(OH)_2$ with a hexagonal structure with diffraction peaks at 19.7°, 33.2°, 38.3°, 52.0°, 59.2°, and 62.8°, ascribed to the (002), (100), (101), (102), (110), and (111) facets of the β-phase nickel hydroxide (JCPDS no: 14-0117), [45] respectively. The similar but relatively weak XRD peaks of BC in the fabricated sample indicate the formation of the BC@$Ni(OH)_2$ composite. XPS measurements were used to further analyze the functional groups of the BC surface during the reaction, and their characteristic peaks of the full survey spectrum are shown in Fig. 3c. Pure BC exhibits two peaks ascribed to the binding energy of the C1s and O1s at ~285.1 and ~532.7 eV, respectively, which were deconvoluted into several peaks, as shown in Fig. S4 (Supplementary Information). The chemical deposition process significantly changed the XPS spectrum, and a typical wide scan of the BC@$Ni(OH)_2$ membrane mainly shows C1s (~285.1 eV), Ni 2p (~856.4 eV) and O1s (~531.4 eV) species, indicating the presence of Ni in the BC substrate [46, 47]. To acquire more detailed information about the changes in the types of bonds, the high-resolution spectra for the Ni 2p peak was investigated (Fig. 3c) to identify two major binding energies at ~853.8 and ~871.8 from Ni $2p_{3/2}$ and Ni $2p_{1/2}$ (Fig. S5, Supplementary Information),[47,48] respectively, which are characteristic to the typical Ni 2p phase of $Ni(OH)_2$. The microscopic and spectroscopic results indicate that $Ni(OH)_2$ architectures were successfully grown on the surface of BC using a chemical deposition process.

The thermal stabilities of BC and the BC@$Ni(OH)_2$ composite were also evaluated. TGA curves for the weight loss plotted as a function of temperature are shown in Fig. 3d. For BC, there were are three distinct decomposition steps: [40] (1) a small weight loss in the first

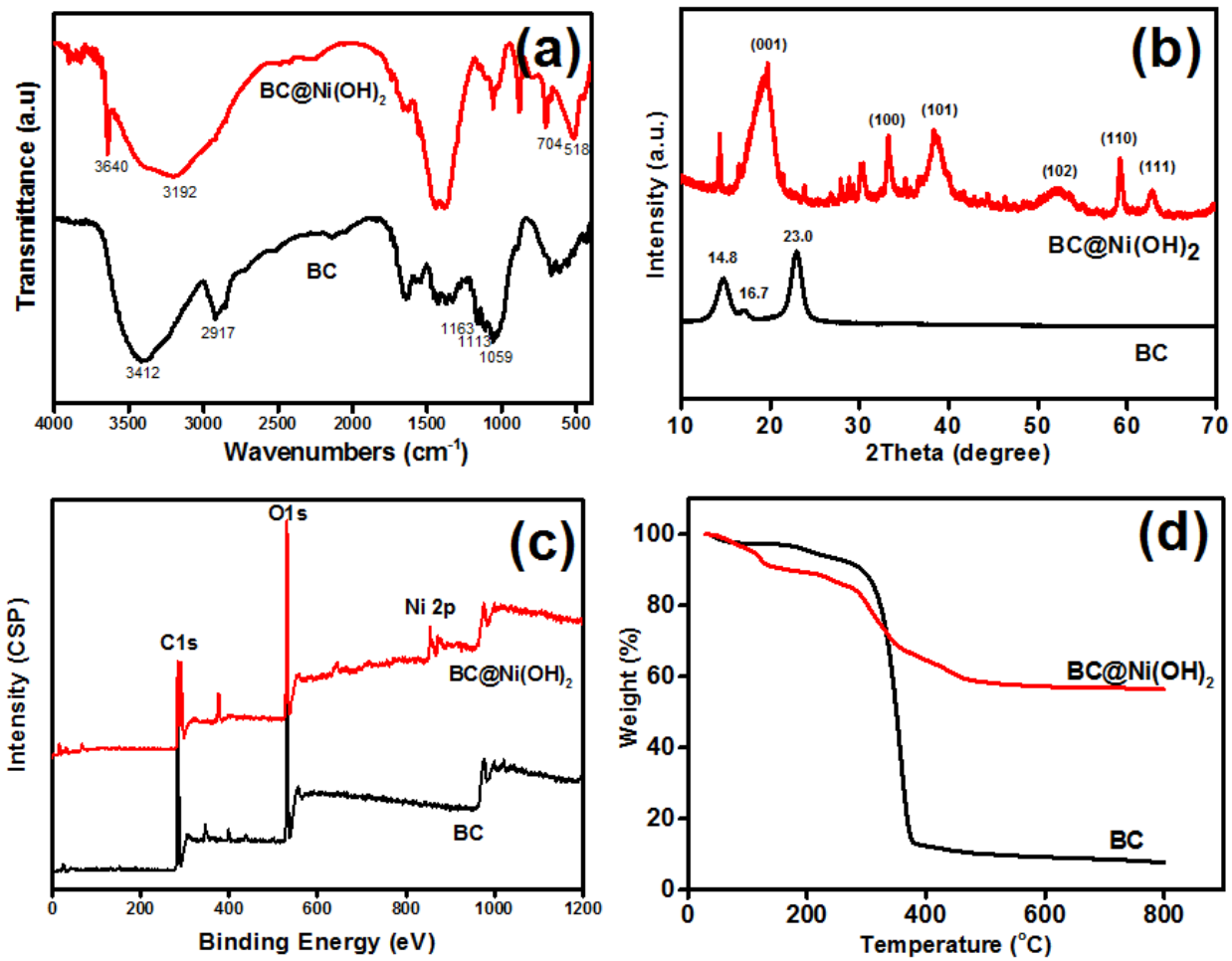

Fig. 3 a) FTIR spectra, b) XRD patterns, (c) XPS survey spectra, and d) TGA curves of BC and the BC@$Ni(OH)_2$ composite.

stage ranging from room temperature to 250 °C, that is assigned to water loss of the cellulose; (2) the second stage (250–380 °C) corresponding to the decomposition of cellulose into d-glucopyranose and free radicals, and (3) the third stage corresponding to the weight loss (380–600 °C), which is due to decarboxylation and decarbonylation reactions. The TGA curves of the BC@$Ni(OH)_2$ composite exhibited similar weight loss behaviors, but the degree of dehydration in the first stage was smaller due to the presence of $Ni(OH)_2$. In the second stage, the BC@$Ni(OH)_2$ composite showed a relative low onset temperature, suggesting a weak thermal stability compared with that of the original BC. In the third stage, the composite had a lower weight loss than BC because of the NiO residue.

The BC@$Ni(OH)_2$ paper can be used directly as freestanding working electrodes for supercapacitor applications without the addition of polymer binders or conductive agents, which was examined using the cyclic voltammetry (CV), galvanostatic charge/discharge (GCD), and electrochemical impedance spectroscopy (EIS) techniques in a three-electrode system in a 6 M KOH aqueous electrolyte (Fig. 4).

During the cathodic and anodic sweeps, CV curves were recorded to characterize the electrochemical behaviors. By comparison, the BC without $Ni(OH)_2$ particles showed negligible capacitance due to the lack of active materials with capacitive features (Fig. 4a). The CV integrated area remarkably increased due to the $Ni(OH)_2$ into BC membranes, and thus, $Ni(OH)_2$ produced enhanced capacitance. Fig. 4b shows the CV curves of the flexible BC@$Ni(OH)_2$ paper electrode at different scan rates. Its capacitance characteristic differs from that of traditional electric double-layer capacitance, evident by the nearly rectangular shape that the CV curves, suggesting that Faradaic processes occur in the electrode material. The redox reaction peaks at the interface of BC@$Ni(OH)_2$ are mainly attributed to the reversible conversion between $Ni(OH)_2$ and NiOOH. The mechanisms correspond to the reaction in different valence states of Ni (+2 and +3) as follows[49]:

$$Ni(OH)_2 + OH^- \rightleftharpoons NiOOH + H_2O + e^-$$

There was no obvious hysteresis between the redox peaks when the scan rate increased from 1 to 50 mV s^{-1}, which indicates that BC@$Ni(OH)_2$ possesses excellent pesudocapacitive characteristics and a good rate performance.

Fig. 4c represents the GCD plots of the as-prepared BC@$Ni(OH)_2$ composite at various current densities for further evaluating its electrochemical properties. The curves with sloped potential plateaus also verify the pseudocapacitive behavior of the BC@$Ni(OH)_2$ electrode, which agrees with the CV curves. Moreover, nearly symmetric nonlinearities were observed in the GCD curves, further suggesting electrochemical reversibility and a rapid I–V response. The areal specific capacitance of the electrode was calculated from the GCD curves by a previously reported method (see Supplementary Information). The calculated specific capacity values were monitored as a function of the current densities and are plotted in Fig. 4d. The gradual decrease in the specific capacitances with the improvement in

current densities is likely related to ion diffusion resistance. At a low current density, the electrolytic ions have sufficient time to permeate into the interior of BC@Ni(OH)$_2$ composite electrode through the deep pores. However, at a high current density or during faster charging, the increased resistance to electrolyte diffusion caused the inner active sites of the composite electrode to be inaccessible for redox reactions. The flexible BC@Ni(OH)$_2$ electrode shows a large specific capacitance of ~2047 mF cm^{-2} at 5 mA cm^{-2}, and retained a capacitance of ~504 mF cm^{-2}, even at a high current density of 30 mA cm^{-2}. This is comparable to that achieved by the current reported metal oxide/hydroxide-based flexible electrodes in an aqueous solution electrolyte (see Table S1 in Supplementary Information). These results reveal the outstanding capacitance behavior and the remarkable rate performance of the BC@Ni(OH)$_2$ composite.

Besides the high specific capacitance, the relationship between the capacitance retention and cycle number by repeated continuous CV scans was also investigated and is shown in Fig. 4e. BC@Ni(OH)$_2$ as a flexible, binder-free electrode exhibited a good cycle life with under 6.0 % capacitance loss after 5000 cycles at a scan rate of 20 mV s^{-1}, which is comparable to the performance of nickel oxide/hydroxide-based electrodes reported in our previous work[50-52]. The electrochemical high-rate performance of the electrode possibly results from the better transportation of electrolytic ions in the electrode material due to the network structure and porous nature. The slight increase in the capacitance at the beginning of cyclic tests can be explained by the activation process, in which more active sites are exposed to the electrolyte.

Furthermore, EIS measurements were conducted to gain a deeper insight into the fundamental behavior of the electrode materials, including the intrinsic ohmic, charge exchange, and ionic resistances. The corresponding Nyquist plot of the BC@Ni(OH)$_2$ membrane electrode exhibited a linear behavior in the low-frequency region and a semi-circle in the high-frequency region, as shown in Fig. 4f. In the low-frequency region, the projected length of the line on the real axis (Z') can be used to evaluate the ion-penetration diffusion process. The line is almost vertical, indicating a pronounced capacitive behavior with short electron transfer and ion diffusion paths in the BC@Ni(OH)$_2$ electrode materials. In the high-frequency region, the solution resistance (R_s) and charge transfer resistance (R_{ct}) can be obtained from the linear and semicircle intercepts with the Z′ axis, respectively. The values of R_s and R_{ct} for BC@Ni(OH)$_2$ were very small, suggesting a low intrinsic resistance of the electrode material, ionic resistance of the electrolyte, contact resistance between the current collector and electrode, and charge interfacial transfer resistance at the electrode/electrolyte.

To investigate the use of the as-fabricated BC@Ni(OH)$_2$ paper as a sensor electrode material, its electrocatalytic activity toward H_2O_2 in an alkaline medium was investigated using CV and chronopotentiometry. Fig. 5a displays the CV behaviors of the BC@Ni(OH)$_2$ electrode in the absence and presence of 1 mM H_2O_2. A peak current was observed after the addition of H_2O_2, which indicates that the BC@Ni(OH)$_2$ composite can be used for sensing H_2O_2. Furthermore, an increase in the current response was achieved by increasing the H_2O_2 concentration, reflecting the high sensitivity of the material to concentration changes of H_2O_2. Here, the sensing mechanism of BC@Ni(OH)$_2$ from the simultaneous reduction of NiOOH and oxidation of H_2O_2 can be described by the following reactions[53]:

$$Ni(OH)_2 + OH^- \rightleftharpoons NiOOH + H_2O + e^-$$
$$2NiOOH + H_2O_2 \rightarrow 2Ni(OH)_2 + O_2\uparrow$$

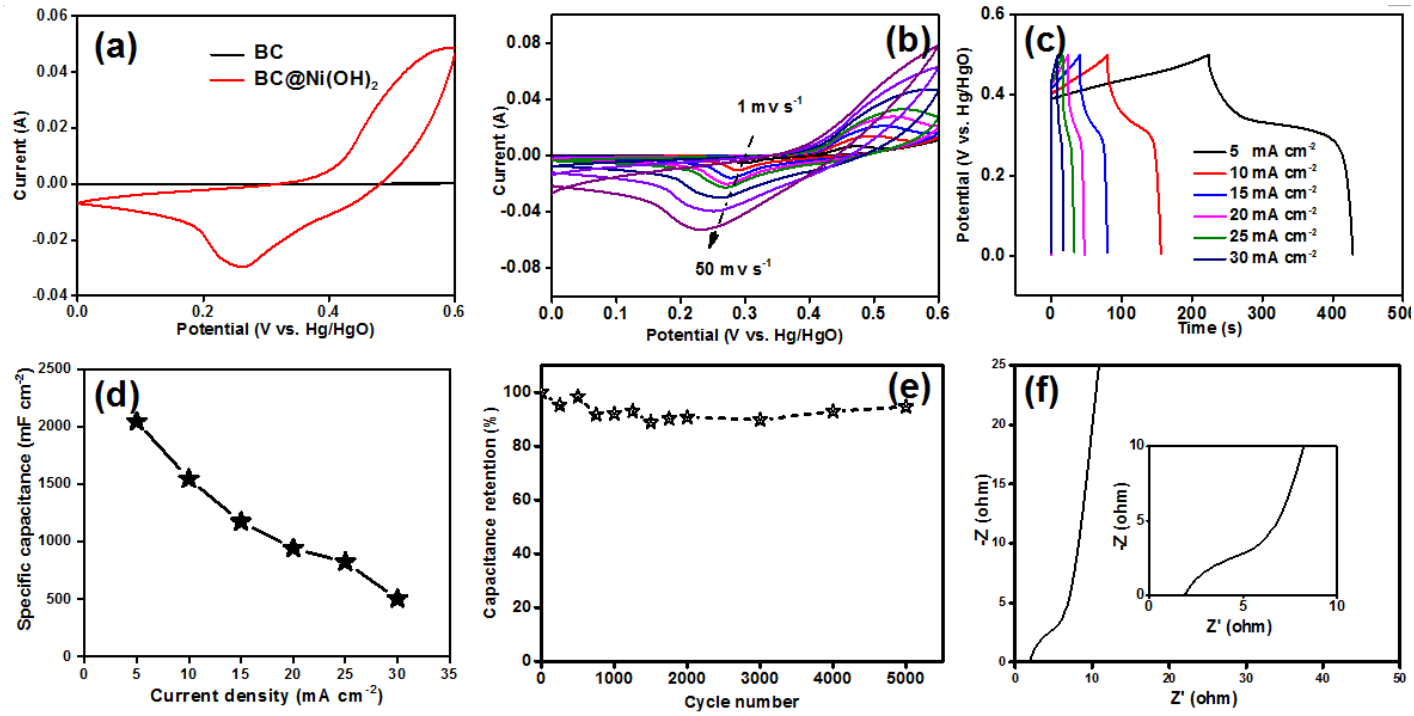

Fig. 4 Electrochemical performance measured in a three-electrode system. (a) Typical CV curves of BC and BC@Ni(OH)$_2$ electrodes at a scan rate of 10 mV s^{-1}, (b) CV curves BC@Ni(OH)$_2$ electrode at different scan rates; (c) GCD curves of BC@Ni(OH)$_2$ electrode at different current densities, (d) specific capacitance of BC@Ni(OH)$_2$ electrode at different current densities, (e) cycling ability of BC@Ni(OH)$_2$ electrode at scan rate of 20 mV s^{-1}; and (f) Nyquist plots of BC@Ni(OH)$_2$ electrode (inset: magnified 0−10 Ω region).

More specifically, the oxidation of Ni^{2+} to Ni^{3+} in solution resulted in the release of electrons. Correspondingly, H_2O_2 was oxidized to O_2 in the presence of Ni^{3+}, resulting in Ni^{2+} formation. Thus, the formation of Ni^{2+} improves the oxidation peak current.

The chronopotentiometric response (Fig. 5b) to successive injection of H_2O_2 was studied to further confirm the electrocatalytic activity of BC@Ni(OH)$_2$. A typical current–time plot exhibited a step-like increase in the current with respect to a stepwise addition of H_2O_2. Also, the quick response of the composite electrode to the added analytes in a short response time is evident from the graph, demonstrating the good electrocatalytic ability and fast and sensitive response. The upper left inset of Fig. 5c shows the corresponding calibration curve for the BC@Ni(OH)$_2$ sensor based on the chronopotentiometric results. It has good linearity (coefficient R^2=0.9995) as the concentration of H_2O_2 increased from 0.1 to 12.4 mM. The sensor (BC@Ni(OH)$_2$) had a low detection limit of 0.28 μM (signal-to-noise ratio, S/N=3) and an optimal sensitivity of 3.79 μA mM^{-1} cm^{-2}. The sensing performance of the fabricated sensor fabricated was compared with other non-enzymatic sensors used for H_2O_2 electroanalysis, as shown in Table S2 (Supplementary Information). It is clear that the BC@Ni(OH)$_2$ electrode exhibited a comparable or slightly better performance compared with the previously reported H_2O_2 sensors. The avoidance of interfering species is also a significant factor for non-enzymatic H_2O_2 sensors. Several common species that can interfere with H_2O_2 detection, uric acid (UA), ascorbic acid (AA), dopamine (DA), Sodium chloride (NaCl), and L-cysteine (L-Cys), were investigated. There was an insignificant current response observed due to the interferents, as shown in Fig. 5d.

Moreover, its reproducibility, repeatability, and stability were also evaluated. The reproducibility was determined by using six individual electrodes in 1 mM H_2O_2, and the relative standard deviation (RSD) of the current response was estimated to be 1.63 % (Fig. 6a). The repeatability was also examined using one electrode to detect 1 mM H_2O_2 seven times, and an RSD of 1.60% was obtained (Fig. 6b). The sensing stability was also tested, showing that the response current after 2000s retained ~89 % of its initial value (Fig. 6c). In addition, when the electrode was tested intermittently over a period of 12 days, good repeatability was observed (Fig. 6d). These results confirmed that the BC@Ni(OH)$_2$ electrode sensor is reliable and reproducible, and is stable enough for use as an electrochemical H_2O_2 sensor.

To further investigate the practical applicability of the present non-enzymatic sensor (BC@Ni(OH)$_2$), the recoveries of analytes were tested with food systems. H_2O_2 is usually used as a preservative in milk. Thus, milk spiked with a certain amount of the H_2O_2 standard solution was selected as the simulated food. In a series of analyses, the recovered H_2O_2 quantities measured by sensor are listed in Table S3 (Supplementary Information), which verified that the synthesized BC@Ni(OH)$_2$ is a promising candidate for real sample sensing. The recovery percent (%R) of the milk samples was performed through the method described in Supplementary Information.

The excellent performance in the electrochemical capacitive behavior and the electrocatalytic oxidation of H_2O_2 might originate from the synergistic effect of the physicochemical properties of BC@Ni(OH)$_2$ hybrid: (1) the unique structure of the fiber network-anchored Ni(OH)$_2$ and the better wettability of the cellulose substrate enhanced the ion, electron, and molecular diffusion transport and decreased the interfacial

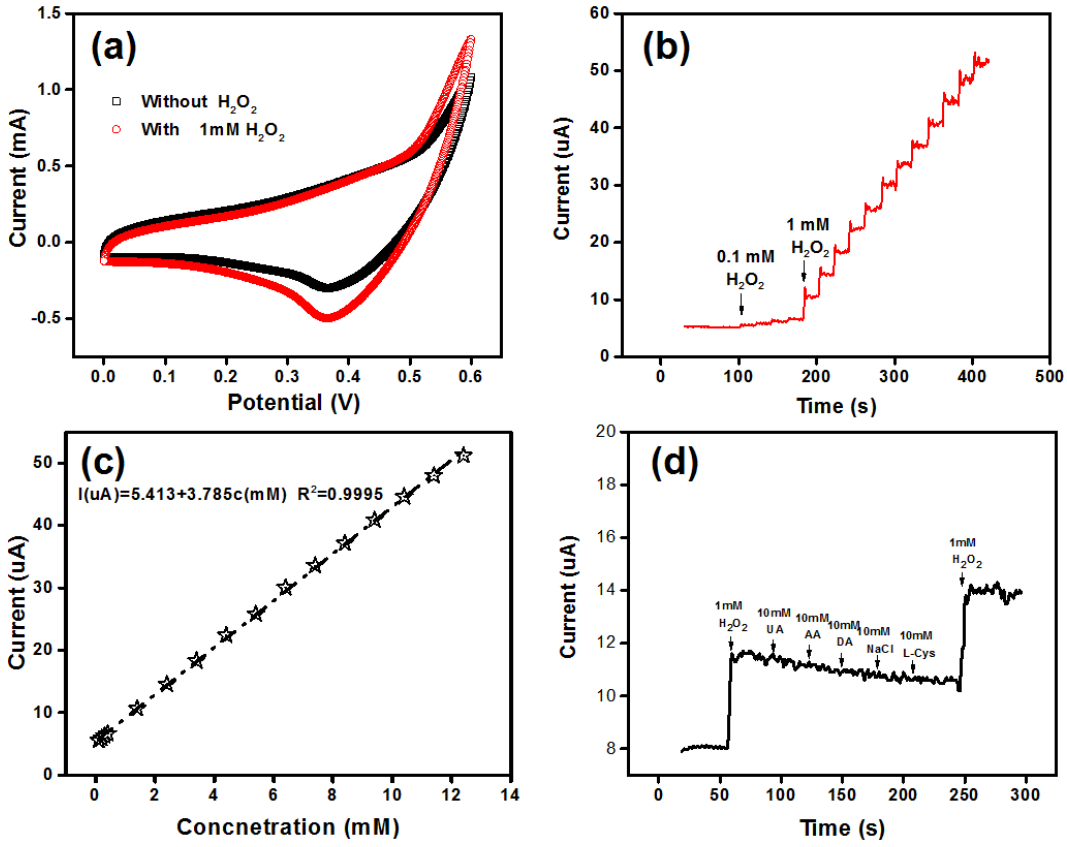

Fig. 5 a) CV profiles of BC@Ni(OH)$_2$ in the presence of 1 mM H_2O_2 recorded at a scan rate of 50 mV s^{-1}, b) chronopotentiometric curves of BC@Ni(OH)$_2$ at different injected concentrations of H_2O_2, c) calibration plot between current and concentration, and d) selectivity test for BC@Ni(OH)$_2$ towards H_2O_2 in the presence of some common interference species such as UA, AA, DA, NaCl, and L-Cys.

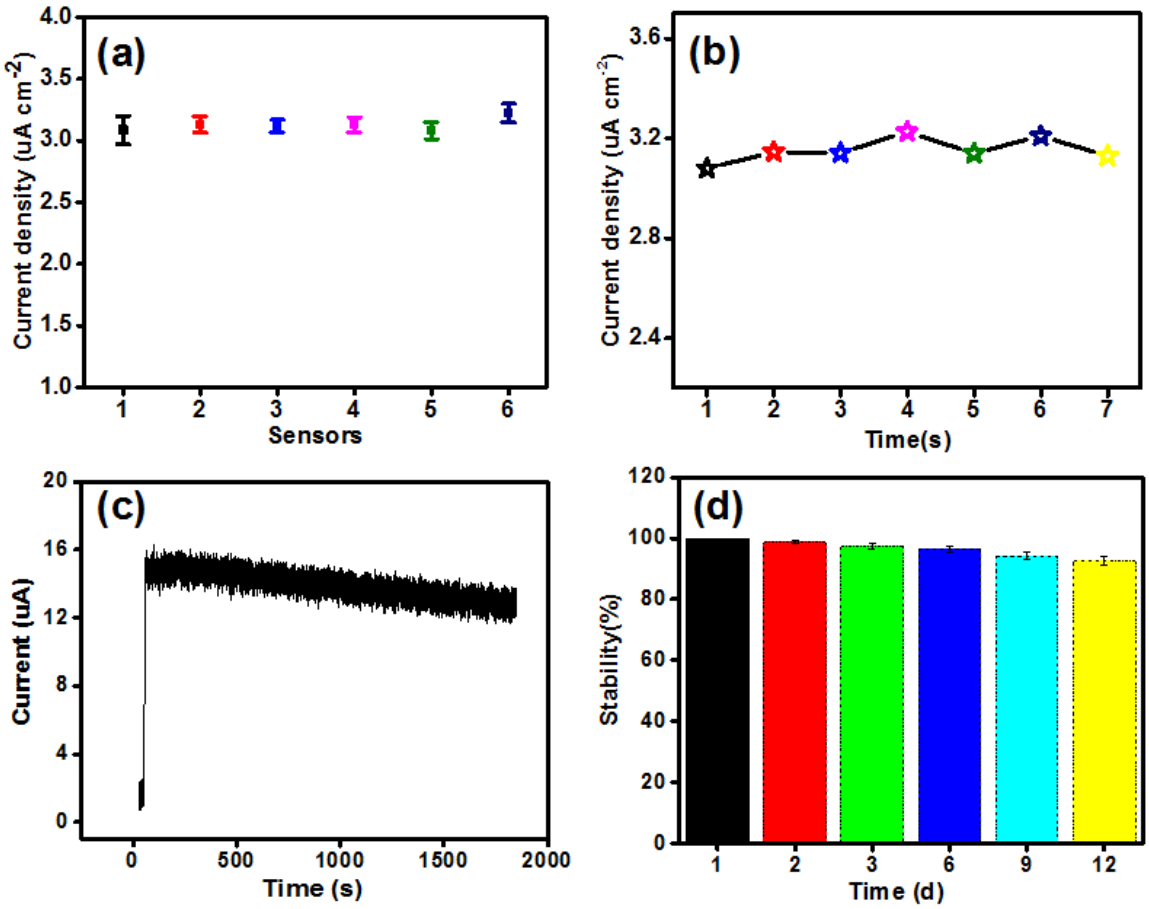

Fig. 6 a) Reproducibility of six BC@Ni(OH)$_2$ electrodes for detection of 1 mM H_2O_2, b) repeatability of BC@Ni(OH)$_2$ electrode for detecting 1 mM H_2O_2 seven times, c) long time amperometric response test for BC@Ni(OH)$_2$ electrode with 1 mM H_2O_2 injection, and d) stability measurement of BC@Ni(OH)$_2$ electrode for 12 days.

and contact resistances; and (2) the small-sized Ni(OH)$_2$ provided enormous active sites for electrochemical reactions. The results clearly indicate that the BC@Ni(OH)$_2$ paper (fabricated by the facile chemical precipitation process presented herein) is a potential flexible electrode for next-generation energy storage devices and highly selective and sensitive sensors.

4. Conclusions

In summary, we successfully demonstrated a facile and scalable method to fabricate BC@Ni(OH)$_2$ paper to achieve a material with a high capacitance and sensitive H_2O_2 detection. The as-prepared composite paper inherits the robust mechanical properties of BC and the high electrochemical performance of Ni(OH)$_2$. These advantages enable the material to achieve an exceptional areal capacitance and good flexibility. The directly presented supercapacitor electrode was characterized by a remarkable areal specific capacitance of ~2047 mF cm^{-2} at a current density of 5 mA cm^{-2} and excellent cycling stability, with 94.6% capacitance retention after 5,000 cycles. Due to its electrocatalytic properties, the fabricated composite paper exhibits a fast response for the non-enzymatic electrochemical detection of H_2O_2 in a linear detection range of 0.1–12.4 mM, with a low detection limit of 0.28 μM, acceptable sensitivity of 3.79 μA mM^{-1} cm^{-2}, excellent selectivity in the presence of common interfering agents, and reliable detection of H_2O_2. The outstanding properties of the composites were obtained due to the synergy of the robust Ni(OH)$_2$/BC hybrid. This research clearly outlines that the BC@Ni(OH)$_2$ paper is a promising material for application in energy storage and non-enzymatic electrochemical sensors.

Acknowledgements

This work has been supported by the Natural Science Foundation of Hubei Province of China (No.2017CFB198) and the Talent Introduction Foundation of Wuhan Polytechnic University (WHPU, China) (No. 2016RZ22). Also, it was partially funded by the Research and Innovation Initiatives of WHPU (No. 2018J01) and National Natural Science Foundation of China (31771925). Dr. Jie Cai thanks the Young Talents Supporting Program of China Association of Science and Technology and the Chutian Scholar Program of Hubei Provincial Government, China.

Conflicts of interest

There are no conflicts to declare.

References

1. W. Xu, J. Lu, W. Huo, J. Li, X. Wang, C. Zhang, X. Gu and C. Hu, *Nanoscale*, 2018, **10**, 14304-14313.
2. P. Ahuja, S. Kumar Ujjain and R. Kanojia, *Appl Surf Sci*, 2017, **404**, 197-205.
3. A. T. E. Vilian, B. Dinesh, M. Rethinasabapathy, S. K. Hwang, C. S. Jin, S. H. Yun and Y. K. Han, *J Mater Chem A*, 2018, **6**, 14367-14379.

4. L. Wang and X. Hu, *Chem-Asian J* 2018, **13**, 1518-1529.
5. S. Xie, S. Liu, P. F. Cheng and X. Lu, *Chemelectrochem*, 2018, **5**, 571-582.
6. V. Strauss, K. Marsh, M. D. Kowal, M. El-Kady and R. B. Kaner, *Adv Mater*, 2018, **30**, 1704449.
7. Y. Liu, C. Li, C. Liu, Y. Chen, K. An and L. Kai, *Carbon*, 2018, **136**, 139-142.
8. Z. Lu, J. Foroughi, C. Wang, H. Long and G. G. Wallace, *Adv Energy Mater*, 2018, **8**, 1702047.
9. Y. Cao, X. Wang, Z. Gu, Q. Fan, W. Gibbons, V. Gadhamshetty, N. Ai and G. Zeng, *J Power Sources*, 2018, **384**, 360-366.
10. J. Cai, H. Niu, H. Wang, H. Shao, J. Fang, J. He, H. Xiong, C. Ma and T. Lin, *J Power Sources*, 2016, **324**, 302-308.
11. L. Jiang, J. Wang, X. Mao, X. Xu, B. Zhang, J. Yang, Y. Wang, J. Zhu and S. Hou, *Carbon*, 2017, **111**, 207-214.
12. X. Jian, H. M. Yang, J. G. Li, E. H. Zhang, L. L. Cao and Z. H. Liang, *Electrochim Acta*, 2017, **228**, 483-493.
13. R. T. Woodward, F. Markoulidis, F. D. Luca, D. B. Anthony, D. Malko, T. O. Mcdonald, M. S. P. Shaffer and A. Bismarck, *J Mater Chem A* 2018, **6**, 1840 -1849.
14. J. Cai, H. Niu, Z. Li, Y. Du, P. Cizek, Z. Xie, H. Xiong and T. Lin, *Acs Appl Mater Interfaces*, 2015, **7**, 14946-14953.
15. Z. Tang, Z. Pei, Z. Wang, H. Li, J. Zeng, Z. Ruan, Y. Huang, M. Zhu, Q. Xue and J. Yu, *Carbon*, 2018, **130**, 532-543.
16. B. Lv, P. Li, Y. Liu, S. Lin, B. Gao and B. Lin, *Appl Surf Sci*, 2018, **437**, 169-175.
17. S. Ravichandran, S. R. S. Raman, S. M. Krishna, S. S. Ravuri, V. Sandhya, S. Ghosh, N. K. Sahu, S. Punniyakoti, M. Karthik and P. Kollu, *Electrochim Acta*, 2018, **276**, 284-292.
18. X. Lu, C. Shen, Z. Zhang, E. Barrios and L. Zhai, *ACS Appl Mater Interfaces*, 2018, **10**, 4041-4049.
19. L. Shao, Q. Wang, Z. Ma, Z. Ji, X. Wang, D. Song, Y. Liu and N. Wang, *J Power Sources*, 2018, **379**, 350-361.
20. R. B. Ambade, S. B. Ambade, N. K. Shrestha, R. Salunkhe, W. Lee, S. S. Bagde, J. H. Kim, Y. Yamauchi, S. H. Lee and F. J. Stadler, *J Mater Chem A*, 2017, **5**, 172-180.
21. A. Alabadi, S. Razzaque, Z. Dong, W. Wang and B. Tan, *J Power Sources*, 2016, **306**, 241-247.
22. Z. Li, J. Cai, P. Cizek, H. Niu, Y. Du and T. Lin, *J Mater Chem A*, 2015, **3**, 16162-16167.
23. D. Hong and S. Yim, *Langmuir*, 2018, **34**, 4249-4254.
24. G. S. Gund, C. D. Lokhande and H. S. Park, *J Alloy Compd*, 2018, **741**, 549-556.
25. F. N. I. Sari, P. R. So and J. M. Ting, *J Am Ceram Soc*, 2017, **100**, 1642-1652.
26. N. Tang, W. Wang, H. You, Z. Zhai, J. Hilario, L. Zeng and L. Zhang, *Catal Today*, 2018, doi.org/10.1016/j.cattod.2018.1003.1024.
27. T. Deng, W. Zhang, H. Zhang and W. Zheng, *Energy Technology*, 2017, **6**, 605-612.
28. V. S. Manikandan, B. R. Adhikari and A. Chen, *Analyst*, 2018, **143**, 4537-4554.
29. H. Bai, C. Wang, J. Chen, Z. Li, K. Fu and Q. Cao, *J Electroanal Chem*, 2018, **816**, 7-13.
30. C. Fu, H. Yu, L. Su, C. Liu, Y. Song, S. Wang, Z. Lin and F. Chen, *Analyst*, 2018, **143**, 2122-2127.
31. H. J. Sismaet, A. J. Pinto and E. D. Goluch, *Biosens Bioelectron*, 2017, **97**, 65-69.
32. G. Maduraiveeran, M. Sasidharan and V. Ganesan, *Biosens Bioelectron*, 2018, **103**, 113-129.
33. L. Li, Y. Zhang, L. Zhang, S. Ge, H. Liu, N. Ren, M. Yan and J. Yu, *Anal Chem*, 2016, **88**, 5369-5377.
34. L. Liang, F. Lan, L. Li, M. Su, S. Ge, J. Yu, H. Liu and M. Yan, *Biosens Bioelectron*, 2016, **82**, 204-211.
35. S. Rana and K. Tamagake, *J. Am. Soc. Hypertens,* 2015, **68**, 31-39.
36. A. Staruschenko, O. Palygin, V. Levchenko, L. C. Evans and A. W. Cowley, *J Am Soc Hypertens* 2015, **9**, e82.
37. R. Rafipour, S. Kashanian and T. F. Abasi, *IET Nanobiotechnol*, 2014, **8**, 196-200.
38. L. Shabnam, S. N. Faisal, A. K. Roy, A. I. Minett and V. G. Gomes, *Electrochim Acta*, 2017, **224**, 295-305.
39. J. Yoon, T. Lee, G. B. Bapurao, J. Jo, B. K. Oh and J. W. Choi, *Biosens Bioelectron*, 2016, **93**, 14-20.
40. S. Peng, L. Fan, C. Wei, X. Liu, H. Zhang, W. Xu and J. Xu, *Carbohyd Polym*, 2017, **157**, 344-352.
41. J. Xu, L. Zhu, Z. Bai, G. Liang, L. Liu, D. Fang and W. Xu, *Org Electron*, 2013, **14**, 3331-3338.
42. F. Zhang, Y. Liu, Y. Cai, H. Li, X. Cai, I. Djerdj and Y. Wang, *Powder Technol*, 2013, **235**, 121-125.
43. S. Yang, X. Wu, C. Chen, H. Dong, W. Hu and X. Wang, *Chem Commun*, 2012, **48**, 2773-2775.
44. A. Casaburi, Ú. M. Rojo, P. Cerrutti, A. Vázquez and M. L. Foresti, *Food Hydrocolloid*, 2017, **75**, 147-156.
45. Y. Tang, Y. Liu, W. Guo, T. Chen, H. Wang, S. Yu and F. Gao, *J Phys Chem C*, 2014, **118**, 24866-24876.
46. X. Li, R. Ding, W. Shi, Q. Xu, D. Ying, Y. Huang and E. Liu, *Electrochim Acta*, 2018, **265**, 455-473.
47. L. Ma, R. Liu, L. Liu, F. Wang, H. Niu and Y. Huang, *J Power Sources*, 2016, **335**, 76-83.
48. L. Chen, L. Liu, Q. Guo, Z. Wang, G. Liu, S. Chen and H. Hou, *Rsc Advances*, 2017, **7**, 19345-19352.
49. Y. Yang, L. Lei, R. Gedeng, F. Huilong, X. Changsheng, F. Xiujun and J. M. Tour, *Acs Nano*, 2014, **8**, 9622-9628.
50. F. Luan, G. Wang, Y. Ling, X. Lu, H. Wang, Y. Tong, X. X. Liu and Y. Li, *Nanoscale*, 2013, **5**, 7984-7990.
51. L. Huang, D. Chen, Y. Ding, Z. L. Wang, Z. Zeng and M. Liu, *ACS Appl Mater Interfaces*, 2013, **5**, 11159-11162.
52. J. X. Feng, S. H. Ye, X. F. Lu, Y. X. Tong and G. R. Li, *ACS Appl Mater Interfaces*, 2015, **7**, 11444-11451.
53. W. Gao, W. W. Tjiu, J. Wei and T. Liu, *Talanta*, 2014, **120**, 484-490.